



First examination of the influence of Y^{3+} ions on the structural, physical and optical properties of strontium phosphate glasses

El Mahdi Bouabdalli¹ · Mohamed El Jouad¹ · Samira Touhtouh¹ · Abdelowahed Hajjaji¹

Received: 10 September 2022 / Accepted: 13 June 2023 / Published online: 30 June 2023
© The Author(s), under exclusive licence to Springer Science+Business Media, LLC, part of Springer Nature 2023

Abstract

Yttrium-ions-doped strontium phosphate-based glasses were prepared by following the classical melt quenching method. This study focuses on discovering the influence of the yttrium dopant on the physical, optical, and structural characteristics of synthesized glasses. The structural analyzes were performed using X-ray diffraction and Fourier transformer infrared. All of the samples examined exhibit an amorphous character, according to XRD. FTIR absorption spectra revealed that the phosphate network was depolymerized, which increased with the level of Y_2O_3 as the metaphosphate units decreased and the pyrophosphate species increased. The measured density values were used to evaluate the physical characteristics of the glasses samples. Density decreased from 2.108 to 2.099 g/cm³, while molar volume values increased from 60.974 to 62.641 cm³/mol when the yttrium concentration content increased from 0.0 to 1.5 mol.%. The optical measurement shows that the band gap for the energy values decreased from 6.528 to 5.754 eV, showing the alteration of the structure of strontium phosphate by an effect of the yttrium content. In addition, it was concluded that the refractive index of the samples increases with the yttrium oxide content and is inversely related to their optical band gap. Moreover, when the number of Y^{3+} ions is increased, the electronic polarizability increases. The improvement of electronic polarizability gives a good medium for non-linear optical applications. The amount of Y^{3+} ions present has a linear connection with the optical basicity of the materials studied. As a result, the studied glass materials could be useful in photonic applications.

Keywords Yttrium · Strontium phosphate glasses · XRD · FTIR spectroscopic · Structural, physical and optical properties · Melt-Quenching method

✉ El Mahdi Bouabdalli
bouabdalli.e@ucd.ac.ma

¹ Laboratory of Engineering Sciences for Energy (LabSIPE), National School of Applied Sciences, Chouaib Doukkali University, 24000 El Jadida, Morocco

1 Introduction

In recent years, glasses made of silicates, germanates, borates, vanadates, mixed lattices of aluminum silicates, phosphates, boron silicate, and others have been the subject of numerous research studies (Bouabdalli et al. 2021; Bouabdalli et al. 2023a, b; Bouabdalli et al. 2022a, b, c, d, e, f, g, h; Elbatal et al. 2014; El Jouad et al. 2020; Mariscal-Becerra et al. 2017; Rada et al. 2011; Ramzi et al. 2016). These glasses have the ability to incorporate a wide variety of chemical compounds as dopants into their structure, and at the same time, these dopants may incorporate significant amounts of rare earth into their own structures, imparting their (optical) characteristics. Phosphate glasses are among those that have been the subject of the most research because of their intriguing characteristics, such as low melting temperature, high thermal expansion coefficient, high transparency, low viscosity, low refractive index, low dispersion, and low phonon energy (Linganna and Jayasankar 2012; Mahdi Bouabdalli et al. 2022; Mariscal-Becerra et al. 2017). This makes them important for many applications such as optical data transmission, sensing, detection, laser technologies, and solar cells (Bouabdalli et al. 2022a, b, c, d, e, f, g, h; Bouabdalli et al. 2022a, b, c, d, e, f, g, h; Li et al. 2016; Linganna and Jayasankar 2012). Furthermore, phosphate glasses are not as effective as borosilicate glasses in vitrifying some nuclear wastes (Bouabdalli et al. 2022d, e, f, g, h, a, b, c; Karaçoban and Özdemir 2012). The vitrification of some nuclear waste is being considered using phosphate glasses. Moreover, as is well known, phosphate glasses are characterized by low chemical durability and high hygroscopic, therefore the addition of heavy metal oxides such as SrO to the phosphate-based glasses network matrix can enhance their physical, chemical durability, and mechanical strength, and increase glass formation capacity (Bouabdalli et al. 2022a, b, c, d, e, f, g, h; Bouabdalli et al. 2022a, b, c, d, e, f, g, h; Deepa et al. 2018; Sidek et al. 1998; Sreedhar et al. 2013). The structure of phosphate glasses is used to determine their characteristics. According to Brow's review, phosphate glasses have a network-like structure made up of phosphor-oxygen tetrahedrons joined by one to three bridging oxygen atoms (BOs) (Brow 2000). The number of bridging oxygen atoms in the PO_4 tetrahedron is expressed as 'n' in the Q^n notation, indicating network connectivity, which is influenced by the composition of glass (Liang et al. 2011). Due to their low processing temperatures (less than 1000 °C) and lower glass transition temperatures, phosphate glasses have attracted the attention of both the technological and scientific domains (Makhkhas et al. 2013; Shih 2004).

According to research on conductivity in on glasses containing rare earth elements, the conductivity of glass decreases as the amount of rare earth ions increases because these ions move slowly and have large masses (Devidas et al. 2008; Gedam and Ramteke 2013).

Due to their high electrical conductivity, elements ranging from lanthanum to actinium are collectively referred to as rare earth elements (17 elements). Scandium and yttrium, in addition to these 15 lanthanides, also show 3+ oxidation states. We have selected yttrium oxide (Y_2O_3) as the dopant for the premade phosphate glasses from the many rare earth elements. Y_2O_3 , one of the rare earth elements, is essential for changing several physical and chemical characteristics of glasses and ceramics. Studies reported that mixing Y_2O_3 with alkaline earth oxides such as SrO in glass composition improves its chemical, thermal, physical, and mechanical properties (Kaur et al. 2011; Singh, Kalia, and Singh 2015). These glasses have applications in the disciplines of photonics, optics, and biomedicine and have been shown to be extremely effective luminescence materials (Bouabdalli et al. 2022a, b, c, d, e, f, g, h; Sadek et al. 2022). Heavy metal oxide-based glass matrices, such as Y_2O_3 , have attracted a lot of attention. This is a result of their characteristics, as well as structural and physical

qualities such as low transformation temperatures, strong infrared transmission, high density, high refractive index, and high thermal expansion. In addition, they can be used to protect nuclear waste from radiation. Singh and al reported that the addition of Y_2O_3 to glasses generally increases their thermal stability (Singh et al. 2007).

In addition, glasses that include yttrium oxide are of special interest since Y_2O_3 has been found to significantly improve applications such as selective internal radiation therapy (SIRT) to treat liver tumors (Riaz et al. 2009, 2010; Salem and Hunter 2006), as well as the endurance and physical qualities of glass (Bouabdalli et al. 2022d, e, f, g, h, a, b, c; Fu and Christie 2017). It is well known that the composition of yttrium aluminosilicate glass used for in situ radiation therapy, with a formulation of 17.1 mol.% Y_2O_3 , 18.9 mol.% Al_2O_3 , and 64.0 mol.% SiO_2 , is very strong and non-resorbable (Erbe and Day 1993; Hyatt and Day 1987). Beta particles (from the Y^{90} isotope), which have a relatively short half-life of 64.2 h, are released when this glass (in the form of solid microspheres) is activated by neutron bombardment (Burrill et al. 2011; Kawashita et al. 2011; Triller et al. 1995).

Incorporating Y^{3+} into the smaller Zr^{4+} crystal lattice helped form stable cubic zirconia polymorphs, which are thus advantageous for dental implants; According to Borgonovo et al., yttrium-stabilized zirconia can be used as a dental implant material (Borgonovo et al. 2012). The use of neodymium-doped yttrium aluminum garnets (Nd: YAG) to cure cancer (Skena et al. 2017). In addition, the function of yttrium oxide nanoparticles for nerve cells has been investigated (Schubert et al. 2006). The Y_2O_3 nanoparticles functioned as antioxidants that can protect cells from cell death induced by oxidative stress. Although its insoluble compounds, such as yttrium oxides, are non-toxic, its water-soluble compounds, such as yttrium chlorides and yttrium nitrates, are regarded as somewhat hazardous (Cochran et al. 1950). According to a study by Dubois et al. on the toxicity of yttrium chloride, nitrate, and oxide in rats, insoluble yttrium oxide (500 mg/kg) exhibited a relatively nontoxic behavior compared to soluble yttrium chloride (450 mg/kg) and yttrium nitrate (350 mg/kg) (DuBois 1956).

The literature has reported on the structural consequences of the addition of Y_2O_3 to silicate glasses. As Y_2O_3 concentrations exceeded 5 mol%, Singh et al. analyzed the structural alterations of lithium borosilicate glasses with the addition of 0 to 15 mol% of Y_2O_3 and demonstrated that Y_2O_3 operated as a network modifier (Singh et al. 2015). Simon et al. studied iron-containing yttrium aluminosilicate glasses using XPS analysis and mentioned that Y_2O_3 functioned as a network modifier oxide in the silicate glass network (Simon et al. 2005). In their study of borosilicate glasses doped with Y_2O_3 , Fayad et al. observed that, especially at concentrations greater than 1% by weight, Y_2O_3 preferred to behave as a network modulator rather than a former network (Fayad et al. 2018). Moreover, the structure of glasses based on yttrium-doped phosphate was simulated using classical molecular dynamics, and Fu et al. found that the depolymerization of the phosphate network caused yttrium oxide to operate as a network modifier (Fu and Christie 2017).

The present work is devoted first to characterizing the structural composition of phosphate glass containing strontium oxide by doping it with yttrium oxide at different concentrations; second, to discover the physical properties of the strontium phosphate glasses doped with various concentrations of yttrium; third, to study the effect of the addition of yttrium content on the optical properties of the prepared glasses.

2 Materials and methods

2.1 Glass preparation

Four different glass formulations based on strontium phosphate in system 65 (P_2O_5)–(35–x) (SrO)–x (Y_2O_3) (where x varied from 0 to 1.5 mol.%) were prepared using the classic melt quenching technique using an ammonium dihydrogen phosphate ($NH_4H_2PO_4$) for P_2O_5 , Strontium carbonate ($SrCO_3$) for SrO, and yttrium chloride (III) ($YCl_3 \cdot 6H_2O$) for Y_2O_3 . The precursors were weighed, combined in an agate mortar, and then transferred to an alumina crucible, which was then placed in a furnace at 120 °C for 24 h to evaporate the water and ammoniac. Finally, the temperature of the furnace was increased to 1100 °C to reach the melt for about 2 h as highlighted in Table 1. The resultant molten glass was then poured onto a steel plate for quenching and left to cool to room temperature. Figure 1 presents the schematic of the synthesis process method used to prepare the desired glasses as reported in (Bouabdalli et al. 2023a, b).

2.2 Characterization technique

2.2.1 Powder X-ray diffraction

XRD analysis was used to explore the amorphous character of each glass formulation. Data were collected using the X-ray diffractometer (Shimadzu model: XRD 6000 using CuK α radiation, $\lambda=0.154$ nm), in the region of 5° to 70°.

2.2.2 FTIR analysis

Infrared spectroscopy of the glass particles was also performed using a Brüker Tensor 27 spectrometer (Brüker Optics, Germany) which was operated in absorbance mode. Spectra were recorded in the range of 400 to 1500 cm^{-1} utilizing a Standard Pike ATR cell (Pike Technologies, Inc., UK). OPUS software version 5.5 was used for the analysis.

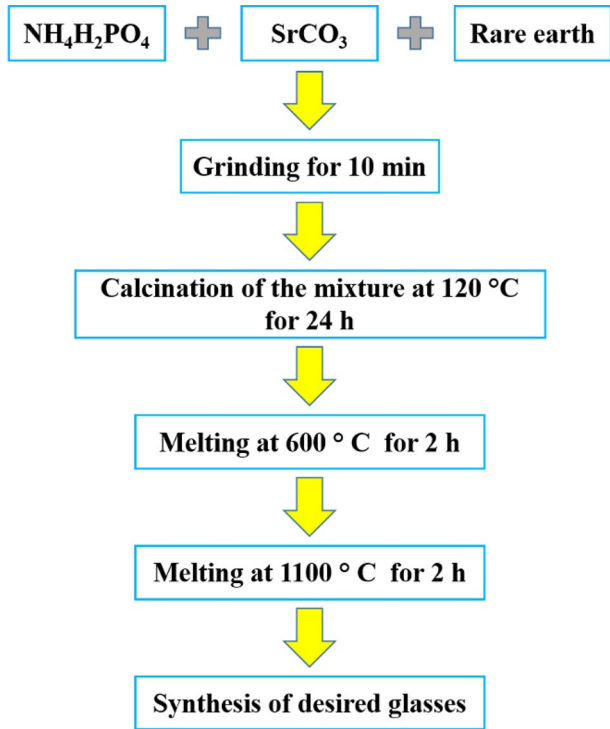
2.2.3 Physical parameters of the studied glasses

The density of pure and yttrium-doped strontium phosphate-based glasses was calculated using the mass/volume formula.

Table 1 Glass codes, drying and melting temperature used throughout the study

Glass code	P_2O_5 content (mol.%)	SrO content (mol.%)	Y_2O_3 content (mol.%)	Drying temp./time (°C/h)	Melting temp./time (°C/h)
PSrY0.0	65	35	0	120/24	1100/2
PSrY0.5	65	34.5	0.5	120/24	1100/2
PSrY1.0	65	34	1	120/24	1100/2
PSrY1.5	65	33.5	1.5	120/24	1100/2

Fig. 1 Schematic illustration of the method used to synthesize the phosphate glasses



$$\rho = \frac{M_T}{V_T} \tag{1}$$

where M_T is the total mass of each glass sample, V_T is the total volume of each glass sample.

The molar volume of the glass of phosphate according to the molecular weight (M) and density yields the following expression (Ahmadi et al. 2017):

$$V_m = \frac{M}{\rho} \tag{2}$$

where V_m is the molar volume and M is the total molecular weight of the multicomponent glasses system given by:

$$M = x_{SrO}Z_{SrO} + x_{P_2O_5}Z_{P_2O_5} + x_{Y_2O_3}Z_{Y_2O_3} \tag{3}$$

where x_{SrO} , $x_{P_2O_5}$, and $x_{Y_2O_3}$ are the mole fractions of the constituent oxides; Z_{SrO} , $Z_{P_2O_5}$, and $Z_{Y_2O_3}$ are the molecular weights of the constituent oxides.

The following quantities such as polaron radius (r_p), ion concentration (N_i), field strength (F), and internuclear distance (r_i) were evaluated by means of the relations.

$$N_i = \frac{N\rho X}{M_{av}} \tag{4}$$

where N is the Avogadro number, X is the mole fraction of the dopant, and M_{av} is the average molecular volume (Ahmadi et al. 2017).

$$r_p(A) = \frac{1}{2} \left(\frac{\pi}{6N_i} \right)^{\frac{1}{3}} \quad (5)$$

Here, N_i is the concentration of the ions.

$$F = \frac{Z}{r^2} \quad (6)$$

Here, r is the radius of the polaron and Z is the atomic number of yttrium.

$$r_i(A) = \left(\frac{1}{N_i} \right)^{1/3} \quad (7)$$

Here, N_i is the concentration of the ions.

2.2.3.1 UV–vis spectral measurements The diffuse reflectance spectra of the glass powders obtained by grinding small glass blocks in a ceramic mortar were collected in the range of 100–1100 nm using a near-infrared UV–Vis spectrophotometer (UV-1800, Shimadzu, El Jadida, Morocco). The spectra were obtained with a resolution of 0.3 nm at room temperature.

The Kubelka–Munk function $F(R)$ has a direct relationship with absorbance. As a result, the following relation was used to convert the $F(R)$ values to the linear absorption coefficient (α):

$$\alpha = \frac{F(R)}{t} \quad (8)$$

where “ t ” is the thickness of the sample.

In the limiting case of an infinitely thick sample, thickness and sample holder have no influence on the value of reflectance (r). In this case, the Kubelka–Munk equation at any wavelength becomes (Yakuphanoglu 2010; Zheng et al. 2011):

$$F(R_\infty) = \frac{(1 - R_\infty)^2}{2R} \quad (9)$$

where $R_\infty = R_{\text{sample}}/R_{\text{standard}}$. The following relational expression proposed by Tauc et al. (Brow 2000; Rada et al. 2012) was used.

$$\alpha h\nu = A(h\nu - E_g)^{\frac{1}{2}} \quad (10)$$

Here, E_g is the band gap, h is Planck’s constant, ν is the vibrational frequency, α is the absorption coefficient, and A is the proportional constant.

The acquired diffuse reflectance spectra were converted to the Kubelka–Munk function. Therefore, the vertical axis was converted to the quantity $F(R_\infty)$, which was proportional to the absorption coefficient. The α in the Tauc equation is substituted with $F(R_\infty)$. Thus, in the actual experiment, the relational expression becomes (Zheng et al. 2011):

$$[F(R\infty)hv]^2 = B(hv - E_g) \quad (11)$$

Therefore, the band gap E_g of a powder sample can be easily extracted by getting $F(R\infty)$ from Eq. (9) and plotting the $[F(R\infty)hv]^2$ against hv .

3 Results and discussions

3.1 XRD analysis

XRD of pure and yttrium-doped strontium phosphate glasses was recorded in the range of 5° to 70° . The results showed that the XRD pattern of the prepared phosphate glasses exhibited extensive diffusion with decreased scattering angles. It showed a long-range structural irregularity, a characteristic of an amorphous nature, as seen in Fig. 2. The XRD characterization graphs, which did not have identifiable or sharp peaks, confirmed that the prepared samples were amorphous. This behavior is consistent with earlier research (Arafat et al. 2020; El-Rehim et al. 2022).

Fig. 2 XRD patterns for glass of the $65 P_2O_5-(35-x) SrO-xY_2O_3$ phosphate system (where $x=0, 0.5, 1, \text{ and } 1.5 \text{ mol.}\%$)

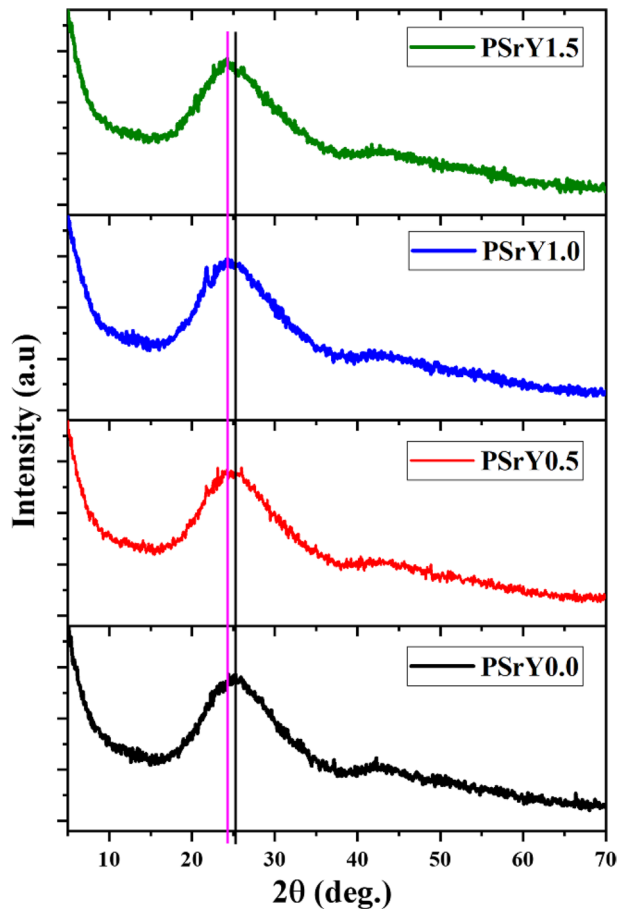
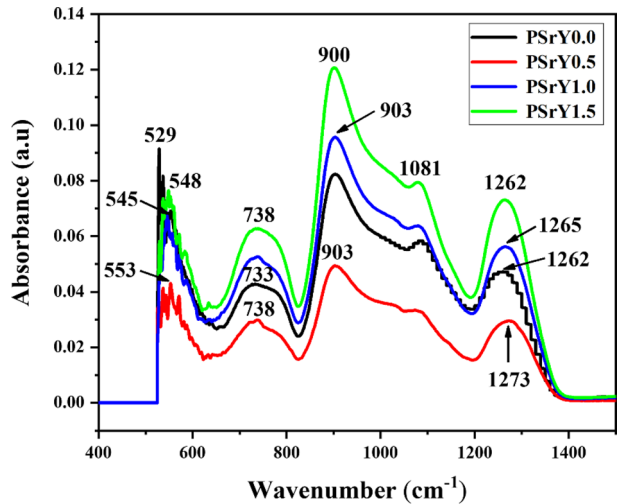


Table 2 The position and full width at half maximum (FWHM) of the XRD broad-halo peak of the strontium phosphate glasses as a function of the yttrium concentrations

Samples	Position broad-halo peak (degree)	FWHM (degree)
PSrY0.0	25.4326	11.00232
PSrY0.5	25.12569	11.73809
PSrY1.0	25.09676	11.60451
PSrY1.5	24.91034	12.12556

Fig. 3 FTIR spectra for strontium phosphate-based glasses in the $65 \text{ P}_2\text{O}_5-(35-x) \text{ SrO}-x \text{ Y}_2\text{O}_3$ system (with $x=0, 0.5, 1$ and $1.5 \text{ mol.}\%$)



The broad halo-peak XRD positions and their full width at half maximum (FWHM) for each of the examined glasses, determined by the origin program, are shown in Table 2. When the dopant impact on the strontium phosphate glass system was compared, it was discovered that, as the concentration of yttrium increases, the position of the XRD broad halo-peak shifts toward lower angles of diffraction, as shown in Table 2 and Fig. 2. Additionally, it has been found that as the amount of yttrium in phosphate glasses rises, so does the FWHM of the XRD broad halo-peak. This behavior may be explicated by the change in interatomic distances due to the yttrium dopant. It is also important to note that the amorphous nature of the glass structure was not affected by the addition of a dopant to the glass system. The results obtained are in good agreement with previous work published in the literature (Omar et al. 2016).

3.2 FTIR analysis

Fourier transform infrared (FTIR) spectroscopy was performed to explore any structural changes within the glasses produced. Figure 3 shows the FTIR spectra of $65 \text{ P}_2\text{O}_5-(35-x) \text{ SrO}-x \text{ Y}_2\text{O}_3$ glasses in the frequency region between 400 and 1500 cm^{-1} . The spectra of the pure and yttrium-doped strontium phosphate glasses have similar spectral features. The FTIR spectra can be deconvoluted using Gaussian lines to the component bands for each one to study the origin of this characteristic FTIR symmetry. Other peaks have been obtained by deconvolution in the $400\text{--}1500 \text{ cm}^{-1}$ wavenumber region. Table 3 lists the

Table 3 The assignments and relative areas of different vibrational bands from FTIR spectra of 65 P_2O_5 –(35– x) SrO – x Y_2O_3 glasses

Frequency regions (cm^{-1})	Assignments	Relative areas dependence of vibrational bands versus Y_2O_3 concentrations (x mol.%)			
		0	0.5	1	1.5
534–548	Network bend	0.75	0.93	1.51	8.46
564–583	Cation oxygen polyhedral and (P_2O_7) $^{4-}$ groups	3.32	1.80	2.79	0.42
721–738	(P–O–P)sym stretch (Q^1)	7.66	4.47	7.81	7.60
902–907	(P–O–P)asym stretch (Q^2)	4.72	2.49	4.95	6.25
1026–1046	(O–P–O)sym stretch (Q^1)	15.79	9.74	18.71	22.37
1269–1277	(O–P–O)asym stretch (Q^2)	4.11	2.95	5.38	6.73

band centers, the relative area of the deconvoluted peaks, and their assignments to the appropriate bands.

The specific deconvoluted spectrum for pure strontium phosphate glass is given in Fig. 4. The band around 534 cm^{-1} is due to the harmonics of the bending vibrations of the O–P–O linkages of basic structural units of phosphate glasses (Ahmed et al. 2004; Doweidar et al. 2005). The wavenumber localized at 564 cm^{-1} is attributed to bending and torsional vibrations that can be assigned to overlapping vibrations involving the strontium oxygen polyhedral and (P_2O_7) $^{4-}$ groups that are characteristic of a structure dominated by Q^1 tetrahedrons (Lai et al. 2012). In addition, at 738 cm^{-1} , there is another band caused by the symmetric stretching vibrations of the P–O–P bridge in the Q^1 units (Sene et al. 2004). Moreover, the strong IR absorbance centered at 907 cm^{-1} is attributed to the asymmetric stretching vibration of the P–O–P links of PO_4 units (Sene et al. 2004). The broad band centered at 1046 cm^{-1} is assigned to the symmetric stretching mode of the O–P–O non-bridging bond in the Q^1 groups (Silva et al. 2010), indicating that the Q^1 units are a completely major component of the structure of the glass of non-doped strontium phosphate.

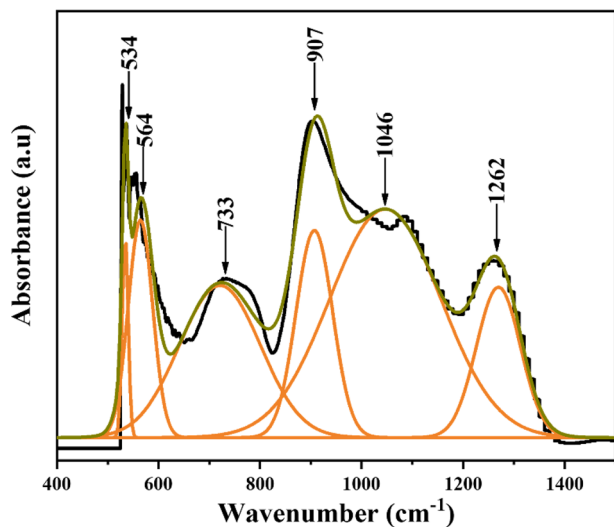
Fig. 4 Deconvoluted FTIR spectra of 65 P_2O_5 –(35– x) SrO – x Y_2O_3 glasses for $x=0$ mol.%

Fig. 5 Deconvoluted FTIR spectra of $65 \text{ P}_2\text{O}_5-(35-x) \text{ SrO}-x \text{ Y}_2\text{O}_3$ glasses for $x=0.5 \text{ mol}\%$

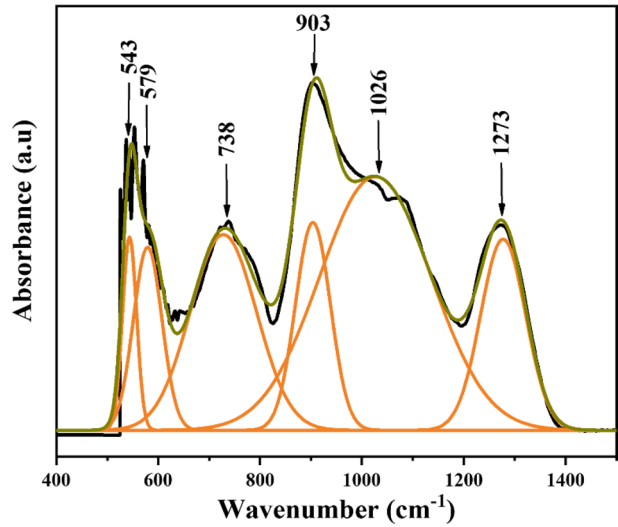
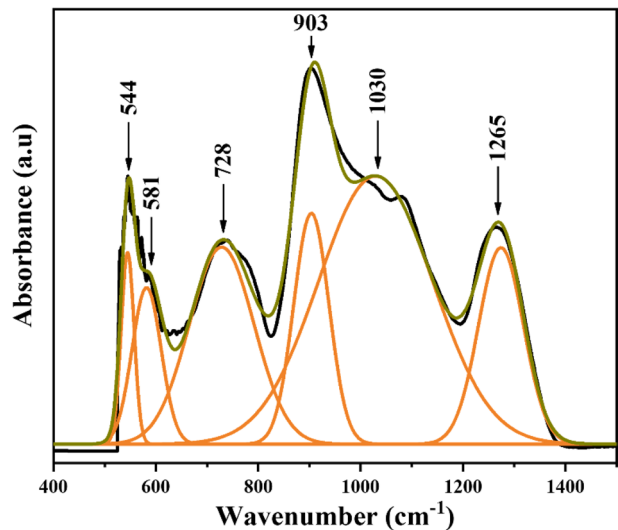


Fig. 6 Deconvoluted FTIR spectra of $65 \text{ P}_2\text{O}_5-(35-x) \text{ SrO}-x \text{ Y}_2\text{O}_3$ glasses for $x=1 \text{ mol}\%$



The absorption band located at 1209 cm^{-1} is attributed to asymmetric stretching motions of the O–P–O non-bridging oxygen in the Q^2 groups (Lu et al. 2015).

As examples represent for the nominal molar composition $0 \leq x \leq 1.5\%$ range, the deconvolution in Gaussian bands of the spectrum for the $x=0.5\%$ and $x=1\%$ glasses, are given in Figs. 5 and 6, respectively. The incorporation of Y_2O_3 into the structural network of the parent-modified strontium phosphate glass is unmistakably shown by changes in the FTIR spectra of $65 \text{ P}_2\text{O}_5-(35-x) \text{ SrO}-x \text{ Y}_2\text{O}_3$ glasses (Fig. 4), which change as the Y_2O_3 content increases. The vibrations of structural units containing Y–O bonds can be observed in the lower frequency section of the FTIR spectra, while structural alterations in the phosphate network are particularly evident in the high-frequency portion of the spectrum. The additions of yttrium content to the base glass result in a change of the absorbance band localized at 733 cm^{-1} to a higher wavenumber (738 cm^{-1}). The shift of

the band was attributed depolymerization of the phosphate network, subsequently reducing the chains and increasing Q¹ pyrophosphate groups. Furthermore, the band localized at 900 cm⁻¹ also showed similar behavior, changing from 900 to 907 cm⁻¹ to characterize the transition from chain to pyrophosphate, increasing the disorder in the glass network (RULMONT et al. 1991). The shift of $\nu_{as}(P-O-P)$ bands toward a higher wave number when the content of the yttrium content increases, a similar trend is observed for the IR spectra for glasses of P₂O₅-CaO-Na₂O-Y₂O₃ when the amount of Na₂O decreases (Arafat et al. 2020). In addition, the position of a prominent band at 1262 cm⁻¹ (produced by the asymmetric stretching of PO₂⁻) is relocated to 1266 cm⁻¹ by adding the amount of yttrium concentrations. Additionally, we notice that as the Y₂O₃ content in the strontium phosphate glasses increases, the location of the IR band's peaks shifts to the lower wavenumber side. It is in line with earlier research (Sene et al. 2008; Shajan et al. 2017).

3.3 Study on physical properties

The physical characteristics of rare-earth-ions-doped strontium phosphate-based glasses depend on the physical glass matrix. The nature and quantity of glass that forms and the network modifier used to affect the physical structure. As a result, the physical characteristics of the glasses examined were calculated using the formula in (Dejneka et al. 1995) and are shown in Table 4. The density measurement of the strontium phosphate-based glasses decreased from 2.108 to 2.099 g/cm³ when the content of the yttrium concentrations increased from 0.0 to 1.5 mol.% as demonstrated in Fig. 7. The reduction in the density of the strontium phosphate glasses can be attributed to the replacement of a larger SrO density (4.7 g/cm³) with a smaller relative density of YCl₃ (2.67 g/cm³). Moreover, a decrease in densities was probably caused by the formation of non-bridging oxygen (NBO) atoms around the doping ions (Aryal et al. 2018; Mohan et al. 2007). With increasing yttrium concentrations, the molar volume of the glasses based on strontium phosphate increased from 60.974 to 62.641 cm³/mol. This increase in the molar volume of the strontium-phosphate-based glasses may be explained by a decrease in the compactness of the glasses. In addition, the increase in volume can be indicated by changes in the structural units of the glass, which can be confirmed by FTIR.

The radius of the polaron shrank as the concentration of trivalent yttrium ions increased, as seen in Table 4. The decrease in the polaron radius as the content of yttrium trivalent ions increased in the strontium phosphate glasses was a signal of decreased deformed lattice sites of the glasses studied. Similarly, as doping

Table 4 Physical properties of yttrium-doped phosphate glasses

Property	PSrY0.0	PSrY0.5	PSrY1.0	PSrY1.5
Density (g/cm ³)	2.108	2.105	2.102	2.099
Average molecular weight (g/mol)	128.530	129.529	130.528	131.526
Molar volume (cm ³ /mol)	60.974	61.530	62.086	62.641
Concentration of Y ³⁺ (Ni, 10 ²⁰ ions/cm ³)	0.0	0.490	0.970	1.442
Polaron radius (r _p , Å)	0.0	11.018	8.771	7.685
Inter-ionic distance (r _i , nm)	0.0	67.770	58.211	53.301
Field strength (F, Å ⁻²)	0.0	0.321	0.507	0.660
Number of bonds per unit volume (n _b , 10 ²⁹ m ⁻³)	0.137	0.136	0.135	0.134

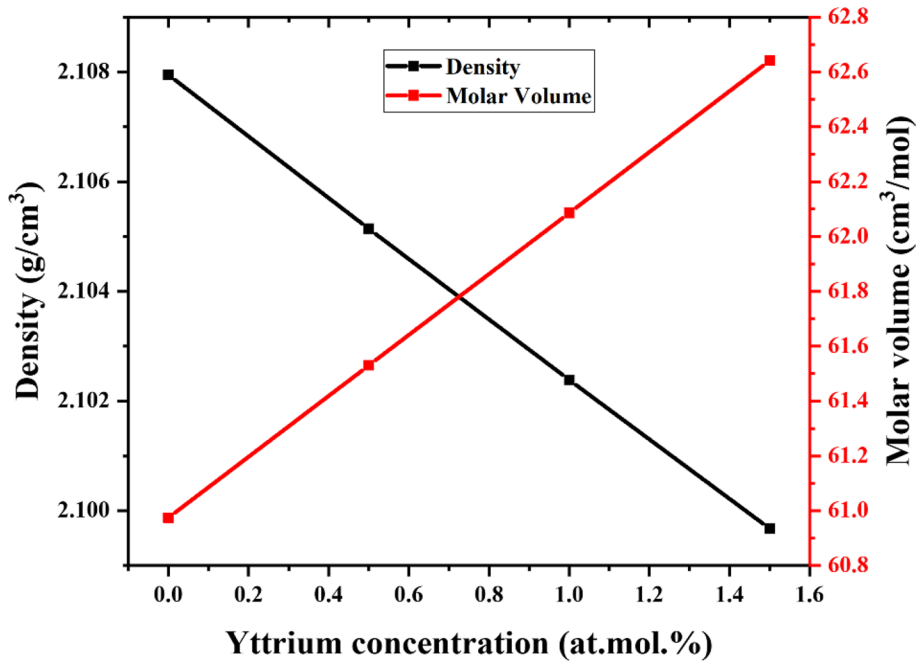


Fig. 7 Change in molar volume and density of the strontium phosphate-based glasses in relation to the yttrium concentration

concentrations increased, the inter-ionic distances between Y^{3+} ions reduced, indicating a rise in the field strength around the ions (Table 4). As doping concentrations increase, attractive forces between ions and the nearby structural elements become stronger, causing field strengths to increase and the inter-ionic distance to decrease (Ramesh et al. 1997). The increased field strength increased as the amount of Y^{3+} ion availability per unit volume increased as the concentration of rare earth ions increased (Fig. 8).

The average phosphorus-phosphorus distance, which may be determined using the formula below, can also be used to study the impact of the yttrium concentration on the phosphate glass system.

$$\langle d_{P-P} \rangle = \left(\frac{V_m}{2N_A(1 - X_P)} \right)^{1/3} \quad (12)$$

where, N_A is the number Avogadro and X_P represents the molar fraction of P_2O_5 . $\langle d_{P-P} \rangle$ is found to vary from 406.72×10^{-02} to 410.02×10^{-02} Å with increasing the content of yttrium.

The oxygen packing density (OPD) and the packing density are also important parameters that explain the system of the glasses. Packing density, V_P (Veeranna Gowda 2013) is the measure of the rigidity of any oxide system that could be determined by the following equation:

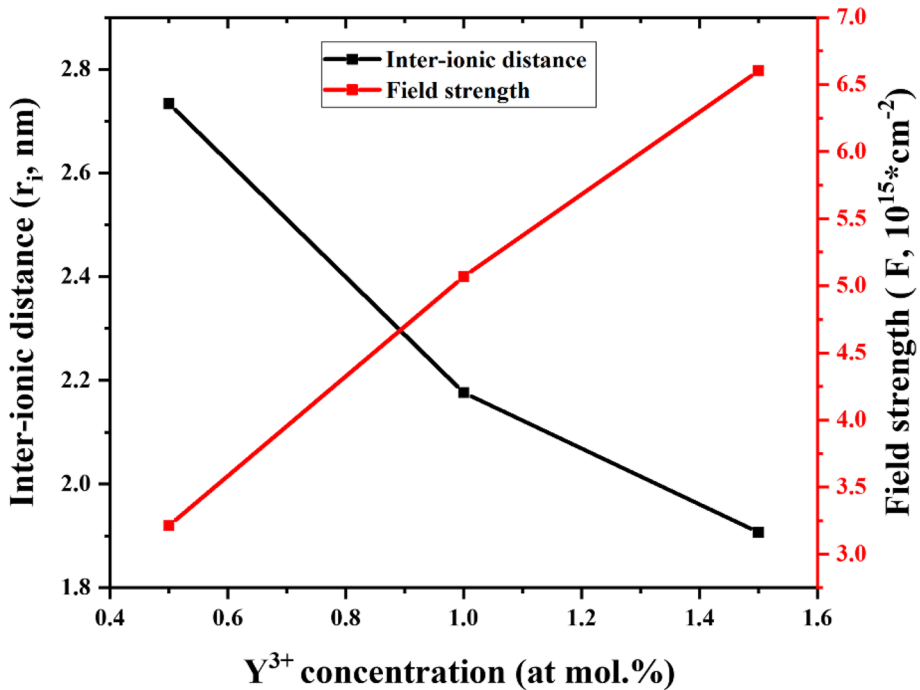


Fig. 8 The variation of the inter-ionic distance and field strength parameters according to the Y^{3+} ion concentrations

$$V_p = \frac{1}{V_m} \sum V_i X_i \tag{13}$$

Here, V_i represents the packing factor and X_i is the mole fraction of the composition. The packing factor (V_i) of an oxide M_XO_Y having M and O ions of ionic radii r_M and r_O can be given by the following relationship:

$$V_i = \frac{4\pi N_A}{3} (X r_M^3 + Y r_O^3) \tag{14}$$

The V_i of $P_2O_5 = 34.8 \text{ cm}^3/\text{mol}$ and $Y_2O_3 = 24.8 \text{ cm}^3/\text{mol}$ are available in the literature (Inaba et al. 1999). For SrO , it is $10.46 \text{ cm}^3/\text{mol}$, calculated in this work via Eq. (10). It is clearly confirmed that the packing density decreases from 0.4293 to 0.4216 with increasing yttrium concentration, increasing the molar volume of the glasses prepared.

The OPD describes the association of oxygen atoms in the glass network, which can be calculated using the formula (Singh et al. 2015). It is discovered that as the yttrium level in the studied phosphate glass increases, the OPD varies between 59.04 and 57.95 mol/l.

The number of bonds per unit volume, n_b , of the glasses can be calculated by the following relationship (Hager and El-Mallawany 2010; Lide 2004):

$$n_b = \sum n_s \frac{N\rho}{M} \tag{15}$$

where n_s is the number of bonds per unit of glass formula, $n_s = (\text{coordination number of each cation}) \times (\text{number of cations in the glass formula unit})$, N represents the number Avogadro, M is the molecular weight of the glass and ρ its density. Table 4 shows the computed values of n_b .

Figure 9 demonstrates the variation observed in the packing density (V_p), $\langle d_{p-p} \rangle$ and the oxygen packing density (OPD) with the change in the composition of yttrium. The formation of additional non-bridging oxygen and small bond modifications are responsible for this change. In addition, the number of bonds per unit of glass volume (n_b) is determined using CN_i , the coordination number of the cations immediately taken from the literature (Lide 2004). The n_b value is observed to decrease as the amount of yttrium in the glass increases, confirming the variance in the molar volume and density values.

3.4 Optical properties

3.4.1 Reflectance spectra

Diffuse reflectance UV–Vis spectra of pure and yttrium-doped strontium phosphate glasses were recorded to characterize their structural features, as shown in Fig. 10. The glass matrices (PSrY0.0) presents the lowest reflectivity in the Ultraviolet region compared to the yttrium-doped glasses and it has the highest reflectivity in the visible region. The Kubelka–Munk transformed reflectance spectra of these prepared glasses are presented in Fig. 11. By extrapolating the linear portion of these spectra to meet the $h\nu$ axis at $[F(R_\infty)h\nu]^2 \rightarrow 0$, the values of the band gap (E_g) have been determined. The optical band gaps as-quenched samples fall in the insulator region. The undoped strontium phosphate glasses (PSrY0.0) exhibit the highest value of the energy band gap around 6.528 eV. When the

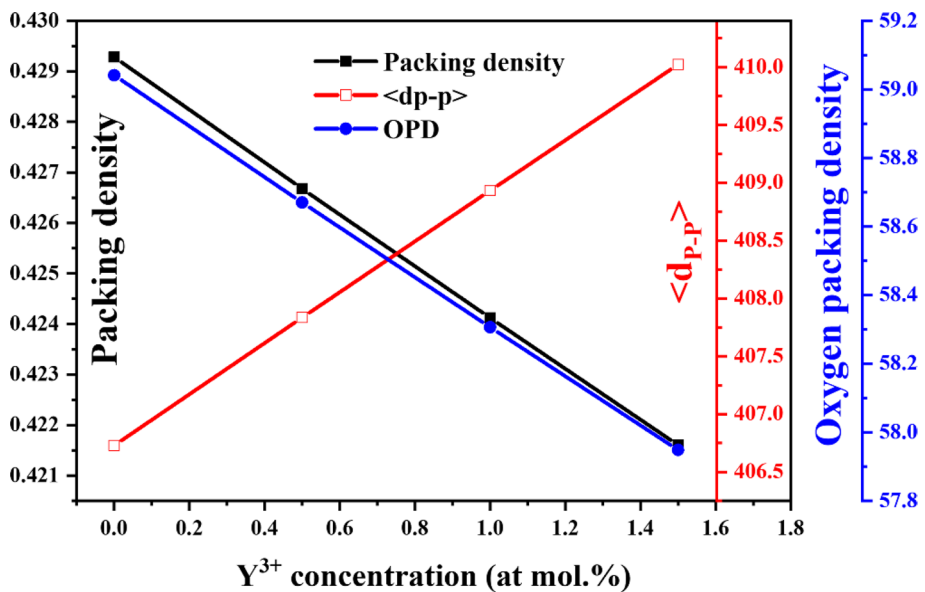


Fig. 9 Variation of packing density, $\langle d_{p-p} \rangle \times 10^{-2} \text{ \AA}$ and OPD (mol/l) with yttrium concentration

Fig. 10 Reflectance spectra of strontium phosphate glasses according to yttrium concentrations

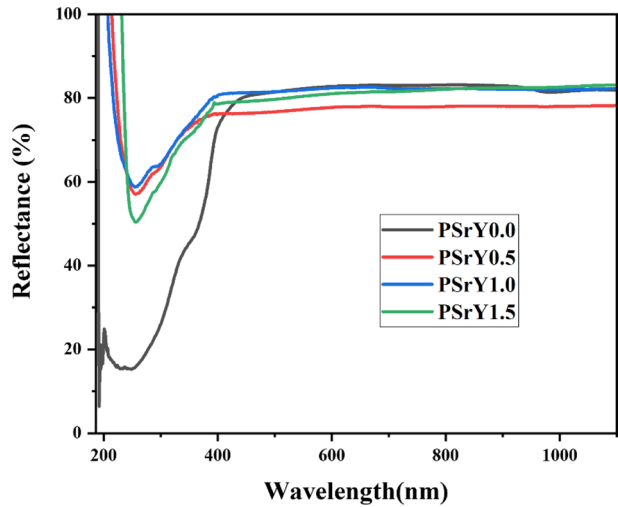
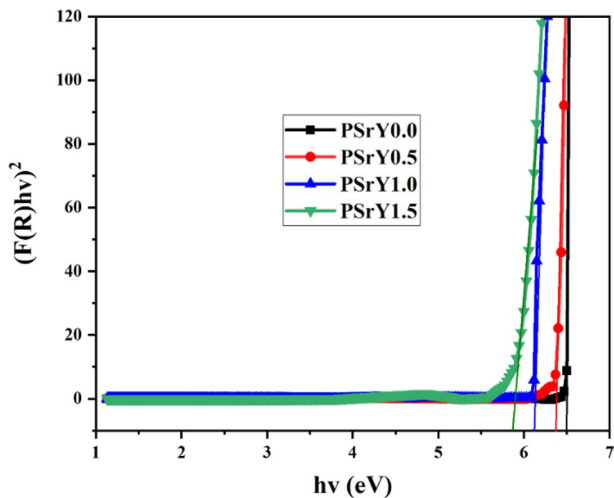


Fig. 11 Energy band gap of the synthesized glasses according to the content of yttrium



yttrium concentration was increased from 0.0 to 1.5 mol.% in strontium phosphate glasses, the optical band gap decreased from 6.528 eV for PSrY0.0 to 5.754 eV for PSrY1.5.

The decrease in the optical band gap of the strontium phosphate glasses with the addition of the yttrium content can be explained by the increase in the non-bridging oxygen, which was reported in previous studies (Novatski et al. 2008; Singh et al. 2015). Moreover, the decrease of the E_{g} values in these yttrium-doped glasses may be due to the increasing cationic field strength (CFS) of the yttrium element (Li et al. 2019). The Urbach energy (E_{u}) of the glass samples was determined using the following relationship:

$$\alpha(\nu) = \beta \exp(h\nu/E_{\text{u}}) \quad (16)$$

The Urbach energy can be obtained from the graph of $\ln F(R)$ versus the photon energy, taking the reciprocal of the slope of the linear portion (Waring and Hsu 1983). The energy

band gap and Urbach energy values are given in Table 5. We observed that the Urbach energy of the synthesized samples increased when the yttrium concentration also increased from 0.0 to 1.5 mol.%. Yttrium is an intermediate oxide that may be employed as both a modifier and a former. In this case, however, it appears to function as a network modulator in the glass phosphate network. In conclusion, the optical band gap and Urbach energy also depend on other factors than non-bridging oxygens (NBOs). The addition of Y_2O_3 leads to a shift in the broad halo peak toward lower diffraction angles, which modifies the glass network. The XRD spectra clearly indicated that the change in the broad halo peak is moving toward lower diffraction angles, where Y_2O_3 is present in glasses. This could be due to the reduction in the length bond and a higher coordination number with oxygens, which exhibits a transformation of the structural unit of the glassy phosphate network from metaphosphate to pyrophosphate and leads to a higher Urbach energy value compared to the PSrY1.5 glass.

3.4.2 Calculation of the refractive index (n) of the prepared glasses

The refractive index (n) for all glass samples in the current study was determined using the following equation (Dimitrov and Sakka 1996; El-Mallawany et al. 2008):

$$n = \left[6 \sqrt{\frac{5}{E_g}} - 2 \right]^{\frac{1}{2}} \quad (17)$$

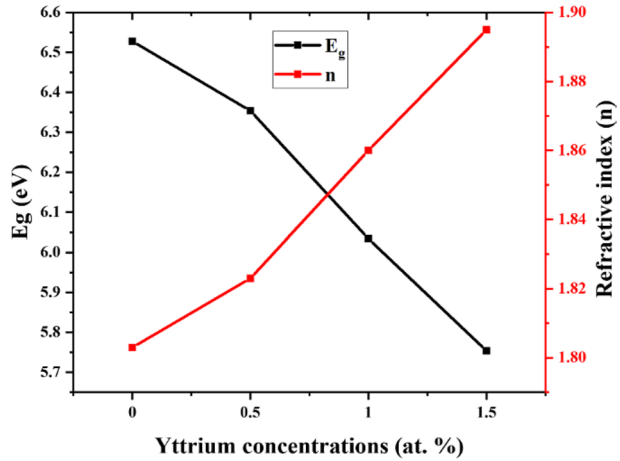
The refractive index (n) values obtained for the prepared glasses are given in Table 5 and presented in Fig. 12. It is clearly observed that the refractive index increased with increasing yttrium content, increasing from 0.0 to 1.5 mol.% in the strontium phosphate glasses.

As demonstrated in Fig. 12, we observed that the value of the refractive indices was oppositely corresponding to the optical band gap of the synthesized samples. The refractive indices obtained are greater than unity and also higher than the index of refraction

Table 5 Optical band gap, Urbach energy, refractive index, molar refractivity, molar polarizability, reflection loss, metallization criterion, electronegativity, electron polarizability, optical basicity and oxide ion polarizability of the pure and yttrium-doped strontium phosphate glasses

Samples	PSrY0.0	PSrY0.5	PSrY1.0	PSrY1.5
Optical band gap (eV)	6.528	6.354	6.034	5.754
Urbach energy (eV)	1.267	2.563	2.750	3.830
Refractive index (n)	1.803	1.823	1.860	1.895
Molar refractivity R_m ($\text{cm}^3 \text{mol}^{-1}$)	26.140	26.850	27.984	29.042
Molar polarizability α_m (\AA^3)	10.362	10.643	11.093	11.513
Reflection loss (R_L)	0.429	0.436	0.451	0.464
Metallization criterion (M)	0.571	0.564	0.550	0.540
Electronegativity (χ)	1.755	1.708	1.622	1.547
Electron polarizability (α^e)	1.921	1.963	2.040	2.108
Optical basicity (^\circ)	0.823	0.846	0.889	0.927
Oxide ion polarizability, $\alpha_{O^{2-}}$ (\AA)	2.881	2.952	3.066	3.173

Fig. 12 The energy band gap (E_g) and the refractive index (n) of the strontium phosphate glasses according to the yttrium content



of silicate glasses, which is approximately 1.458 (Naftaly and Miles 2007). Moreover, the glass samples have a high value (n), which indicates that they can be used as promising materials for photoelectronic and optical filter systems (Rammah et al. 2020). In addition, the increase in the refractive index (n) may be explained by the role of yttrium oxide in altering the structural properties of the strontium phosphate glass system. The addition of trivalent yttrium leads to the modification of the glass matrix by converting the metaphosphate unit to the pyrophosphate unit, which was previously confirmed by FTIR spectroscopy. The conversion of a structural unit of a glass system leads to the creation of non-bridging oxygen, which increases the polarizability of the phosphate glass network. The high polarizability of the lone pair in non-bridging oxygen causes an increase in the refractive index. The formation of non-bridging oxygen leads to the creation of ionic bonds, which increase the number of refractive indices.

The molar refractive (R_m), molar polarizability (α_m) and reflection loss (R_L) can be evaluated by the following relationship (Shaaban et al. 2020):

$$R_m = V_m \left(1 - \sqrt{E_g/20} \right) \tag{18}$$

The molar polarizability (α_m) is directly proportional to the molar refractivity (R_m) of the material by the following equation:

$$\alpha_m = \left(\frac{3}{4\pi N_A} \right) R_m \tag{19}$$

where N_A is the number Avogadro.

The reflection loss (R_L) can be determinate through the ratio between the molar volume (V_m) and the molar refractivity (R_m):

$$R_L = \left(\frac{R_m}{V_m} \right) \tag{20}$$

The molar refractivity (R_m) of a substance is determined by its molar polarizability (α_m). The values obtained for the refractive molar (R_m), molar polarizability (α_m), and reflection loss (R_L) are given in Table 5. It was discovered that (see Table 5) the values of

(R_m), (α_m) and reflection loss (R_L) increase as the Y_2O_3 content increases. These values are increasing as a result of an increase in molar volume.

Electronic oxide ion polarizability, $\alpha_{O^{2-}}$ can be calculated using the obtained molar volume (V_m) and the refraction index (n) of the following relationship reported in (Moss 1985):

$$\alpha_{O^{2-}} = \left[\left(\frac{V_m}{2.52} \right) \left(\frac{n^2 - 1}{n^2 + 2} \right) - \sum_{cat} \alpha \right] / N_{O^{2-}} \quad (21)$$

where $\alpha_{O^{2-}}$ represents the electronic oxide ion polarizability, $\sum \alpha_{cat}$ represents the molar cation polarizability, $N_{O^{2-}}$ is a symbol for the quantity of oxide ions, V_m is the molar volume and n is the refractive index of the glass sample. For a glass with matrix $xA_aO_b - yB_cO_d - zC_eO_f - tD_gO_h$, $\sum \alpha_{cat}$ will be $xa\alpha_A + yc\alpha_B + ze\alpha_C + tg\alpha_D$ and $N_{O^{2-}}$ will be $xb + yd + zf + th$. From the available literature, the values of α_P , α_{Sr} and α_Y are 0.021, 0.861 and 0.554 \AA^3 , respectively (Dimitrov and Komatsu 1999). The values obtained for the electronic oxide ion polarizability for all glass samples are listed Table 5. As can be seen in Table 5, the electronic polarizability of oxide ions increases when the concentration of trivalent yttrium ions is added to the strontium phosphate glasses. The compositional dependence of the molar polarizability and oxide ion polarizability of prepared glasses on the concentrations of yttrium is presented in Fig. 13. As the concentration of trivalent yttrium increases, the increasing trend of molar polarizability of the glass samples is visible. The amount of non-bridging oxygen that is present in the phosphate glass affects the

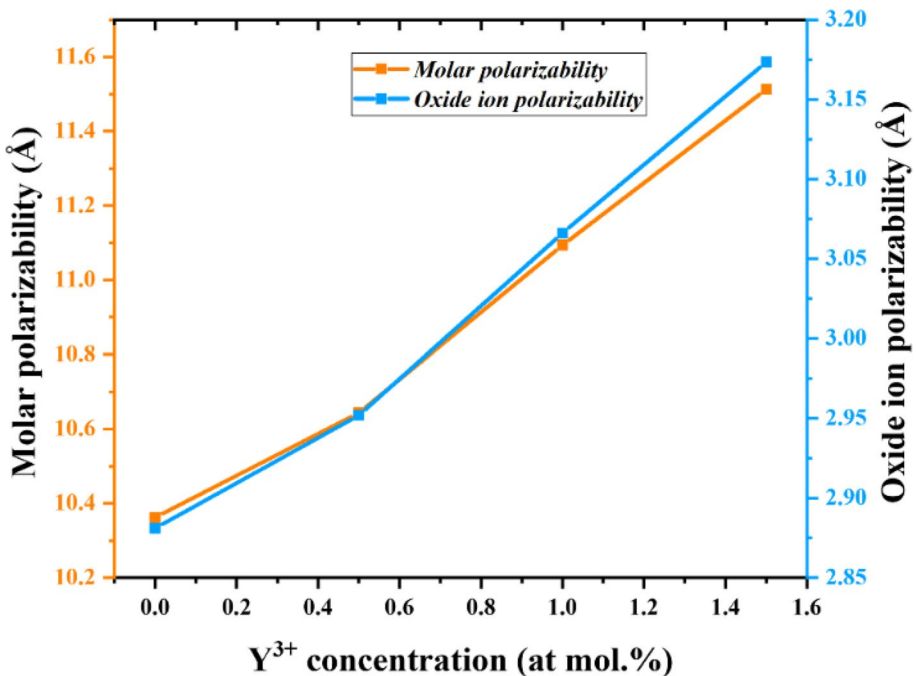


Fig. 13 Molar polarizability and oxide ion polarizability as a function of the yttrium content in the prepared glass

deformability of the electron cloud. Non-bridging oxygen is made up of lone pair free electrons that are less strongly coupled to the nuclear charge. Therefore, free electrons are readily polarized as the electrical field penetrates the material (Halimah et al. 2019). As the concentration of the yttrium trivalent (Y^{3+}) increases, so does the quantity of non-bridging oxygen ions. An increase in the amount of non-bridging oxygen in the glass system causes an increase in the number of free electrons. As a result, as the concentration of Y^{3+} increases, so does the molar polarizability. As can be demonstrated in Fig. 13, we have observed the linear trend of the polarizability of the values of the oxide ions, which are found in the glass samples. The undoped strontium phosphate glasses present the lowest value of the electronic oxide ion polarizability. We have found that the values of oxide-ion polarizability increase when the concentration of yttrium increases from 0.0 to 1.5 mol.% in glass systems. In the past, we hypothesized that a rise in the refractive index causes a rise in the polarizability of oxide ions. This is because there is a direct correlation between the polarizability of oxide ions and molar refraction (Duffy and Ingram 1971).

The metallization criterion of glass samples can be evaluated using the following relationship:

$$M = 1 - \frac{R_m}{V_m} \quad (22)$$

The values of the metallization criteria (M) are directly dependent on the reflection loss (R_L); according to the data in Table 5 and plotted in Fig. 14, it can be seen that M decreases with the addition of yttrium content. This decrease in M shows the metallization of the

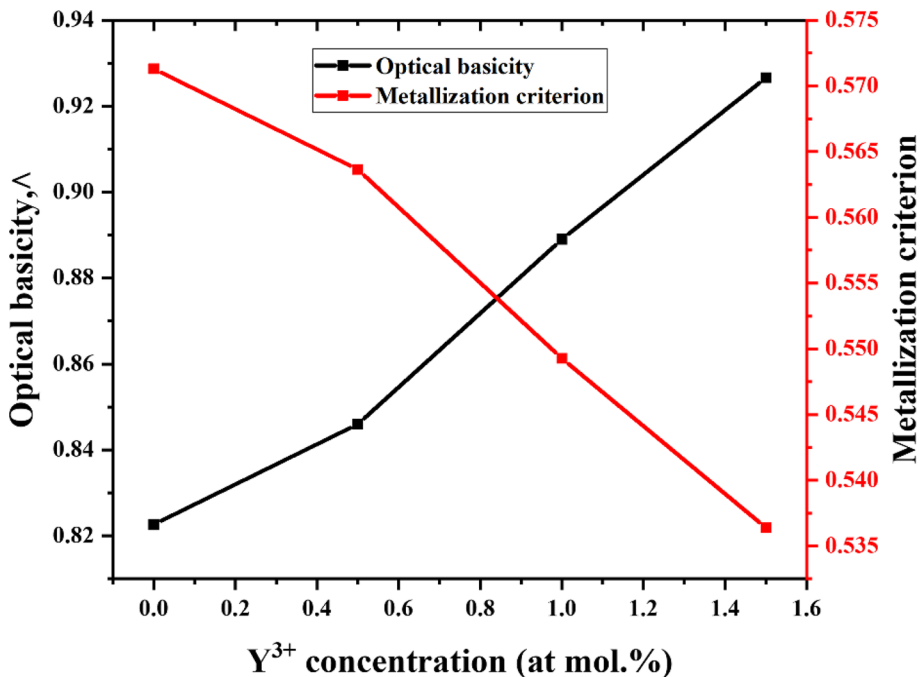


Fig. 14 Optical basicity ($^{\wedge}$) and metallization criterion (M) of the synthesized glasses with different concentrations of yttrium

strontium phosphate-based glass samples, which leads to a decrease in the optical band gap. Therefore, the energy band gap of the phosphate glass affects the metallization criteria. The decreasing value of the energy band gaps suggests that the valence and conduction bands have widened. The glass system will become metalized as a result of this process (Azlan et al. 2019).

The optical electronegativity (χ), the electron polarizability (α°), and optical basicity (Λ) can be estimated using the following equations:

$$\chi = 0.2688 \times E_g \quad (23)$$

$$\alpha^\circ = -0.9\chi + 3.5 \quad (24)$$

$$\Lambda = -0.5\chi + 1.7 \quad (25)$$

The electronegativity (χ) of the glass samples can be calculated using the values of (E_g) (see Table 5). Therefore, the values of electronegativity (χ) decrease with increasing yttrium concentration. Because electronic polarizability and optical basicity follow the opposite trend of electronegativity (χ), their values increase as the concentration of yttrium increases.

Figure 14 also shows the change in optical basicity according to the yttrium content in strontium phosphate glasses. The high value of the optical basicity of the glass series shows that the phosphate glass system is more basic. As a Lewis base in the glass system, oxygen ions lend electrons to the nearby cations. The high degree of donating capacity of oxide ions strongly influenced the property of acid–base. Moreover, the polarization state of the oxide ions in the glass system has been said to be connected to their optical basicity (Duffy 1989). The linear trend of optical basicity along with the concentration is found in the prepared glass. In addition to that, the values of optical basicity are shown to increase somewhat with increasing concentration of Y^{3+} . This behavior can be explained by comparing the optical basicity value of a single element in the phosphate glass system. Former oxides should be less basic than modifier oxides in glass former and modifier conditions. When modifier oxide is added to the former oxide, the modification reaction becomes an acid–base reaction in which modifier oxide ions approach the acidic area of the former oxide in decreasing order of acidity (Sidek et al. 2004).

4 Conclusion

In summary, we successfully prepared pure and yttrium-doped strontium phosphate glasses using the conventional melt-quenching method. The structural properties of the strontium phosphate-based glasses were examined by X-ray diffraction (XRD) and Fourier transform infrared (FTIR) spectra. The X-ray diffraction (XRD) pattern revealed that all of the prepared glasses were amorphous. FTIR spectroscopy shows that the addition of the yttrium content leads to depolymerization of the structural composition of the glass system network, reducing the number of metaphosphate chains and increasing the number of pyrophosphate groups. When the amount of yttrium in the sample glass increased, it was discovered that the density increased from 2.108 to 2.099 g/cm³ and the molar volume reduced from 60.974 to 62.641 cm³/mol. The optical measurement confirmed that the energy band gap of synthesized glasses decreases

with increasing yttrium content. The index of refractive of the sample glass is found to increase with Y₂O₃ supporting the creation of non-bridging oxygen, which increases the polarizability of the phosphate glass network. We have obtained that the molar polarizability values of strontium phosphate glasses increase with increasing concentration of Y³⁺ (1.921–2.108 Å³). The results obtained for the oxide ion polarizability of strontium phosphate glasses are found to be linear in trend along with the Y³⁺ concentration (2.881–3.173 Å). With increasing concentrations of Y³⁺, the linear trend of optical basicity is observed in the strontium phosphate glass system (0.823–0.927). In addition, the value of the metallization criterion of strontium phosphate glass decreased with the content of yttrium (0.571 to 0.540). All of the results of all of the structural, physical, and optical analyzes are in good relation to each other and suggest that these prepared glasses are promising materials for photoelectronic and optical filters.

Author contributions EMB: Conceptualization, formal analysis, methodology, writing-original draft, writing-review & editing. MEJ: Supervision, Validation. ST: Supervision, Validation. AH: Supervision.

Funding El Mahdi Bouabdalli would like to express his deep gratitude to the National Center of Scientific and Technological Research (CNRST), Rabat/Morocco for the funding of his doctoral scholarship (Pre-Doctoral Grants 2019).

Data availability This section does not apply to this study.

Declarations

Competing interests The authors declare that they have no known competing financial interests or personal relationships that could have appeared to influence the work reported in this paper.

Ethical approval Not applicable for this study.

References

- Ahmadi, F., Hussin, R., Ghoshal, S.K.: Structural and physical properties of Sm³⁺ doped magnesium zinc sulfophosphate glass. *Bull. Mater. Sci.* (2017). <https://doi.org/10.1007/s12034-017-1462-5>
- Ahmed, I., Lewis, M., Olsen, I., Knowles, J.C.: Phosphate glasses for tissue engineering: Part 1. Processing and characterisation of a ternary-based P2O5-CaO-Na2O glass system. *Biomaterials* **25**(3), 491–499 (2004). [https://doi.org/10.1016/S0142-9612\(03\)00546-5](https://doi.org/10.1016/S0142-9612(03)00546-5)
- Arafat, A., Samad, S.A., Titman, J.J., Lewis, A.L., Barney, E.R., Ahmed, I.: Yttrium doped phosphate-based glasses: structural and degradation analyses. *Biomed. Glasses* **6**(1), 34–49 (2020). <https://doi.org/10.1515/bglass-2020-0004>
- Aryal, P., Kesavulu, C.R., Kim, H.J., Lee, S.W., Kang, S.J., Kaewkhao, J., Chanthima, N., Damdee, B.: Optical and luminescence characteristics of Eu³⁺-Doped B₂O₃:SiO₂:Y₂O₃:CaO glasses for visible red laser and scintillation material applications. *J. Rare Earths* **36**(5), 482–491 (2018). <https://doi.org/10.1016/J.JRE.2017.09.017>
- Azlan, M.N., Halimah, M.K., Suriani, A.B., Azlina, Y., El-Mallawany, R.: Electronic polarizability and third-order nonlinearity of Nd³⁺ doped borotellurite glass for potential optical fiber. *Mater. Chem. Phys.* **236**, 121812 (2019). <https://doi.org/10.1016/J.MATCHEMPHYS.2019.121812>
- Borgonovo, A.E., Fabbri, A., Vavassori, V., Censi, R., Maiorana, C.: Multiple teeth replacement with endosseous one-piece yttrium-stabilized zirconia dental implants. *Med. Oral Patol. Oral Cir. Bucal* **17**(6), e981 (2012). <https://doi.org/10.4317/medoral.18194>
- Bouabdalli, E.M., El Jouad, M., Garmim, T., Touhtouh, S., Louardi, A., Monkade, M., Hartiti, B.: Preparation and characterization of nickel and aluminum-codoped SnO₂ thin films for optoelectronic applications. *Int. J. Photoenergy* (2021). <https://doi.org/10.1155/2021/5556441>

- Bouabdalli, E.M., El Jouad, M., Touhtouh, S., Hajjaji, A.: First examination of the influence of Y^{3+} ions on the structural physical and optical properties of strontium phosphate glasses. *Res. Square* (2022a). <https://doi.org/10.21203/rs.3.rs-2052185/v1>
- Bouabdalli, E.M., El Jouad, M., Garmim, T., Louardi, A., Hartiti, B., Monkade, M., Touhtouh, S., Hajjaji, A.: Elaboration and characterization of Ni and Al Co-doped SnO_2 thin films prepared by spray pyrolysis technique for photovoltaic applications. *Mater. Sci. Eng. B* **286**, 116044 (2022b). <https://doi.org/10.1016/J.MSEB.2022.116044>
- Bouabdalli, E.M., El Jouad, M., Gaumer, N., Touhtouh, S., Hajjaji, A.: Structural, optical behavior and Judd-Ofelt analysis of Europium-doped silicophosphate glasses for red-emitting device applications. *J. Lumin.* (2022d). <https://doi.org/10.1016/J.JLUMIN.2022.119640r>
- Bouabdalli, E.M., El Jouad, M., Touhtouh, S., Hajjaji, A.: First investigation of the local environment of europium in a strontium phosphate glass using molecular dynamics simulations. *Phosphorus Sulfur Silicon Relat. Elem.* (2022g). <https://doi.org/10.1080/10426507.2022.2136670>
- Bouabdalli, E.M., El Jouad, M., Gaumer, N., Siniti, M., Touhtouh, S., Hajjaji, A.: Structural, physical, thermal and optical spectroscopy studies of the europium doped strontium phosphate glasses. *Inorg. Chem. Commun.* **151**, 110563 (2023a). <https://doi.org/10.1016/J.INOCHE.2023.110563>
- Bouabdalli, E.M., El Jouad, M., Touhtouh, S., Hajjaji, A.: First investigation of the effect of strontium oxide on the structure of phosphate glasses using molecular dynamics simulations. *Comput. Mater. Sci.* **220**, 112068 (2023b). <https://doi.org/10.1016/J.COMMATSCI.2023.112068>
- Bouabdalli, E.M., El Jouad, M., Garmim, T., Louardi, A., Monkade, M., Touhtouh, S.: Elaboration and characterization of Ni and Al Co-Doped SnO_2 thin films prepared by spray pyrolysis technique for photovoltaic applications. Available SSRN 4141072, 1–23, 20 June (2022c) <https://doi.org/10.2139/ssrn.4141072>
- Bouabdalli, E.M., El Jouad, M., Gaumer, N., Touhtouh, S., Hajjaji, A.: Photoluminescence and Judd-Ofelt analysis of europium containing in a strontium phosphate glasses for photonic application. Available at SSRN 4292770, 1–27 (v) (2022e). <https://ssrn.com/abstract=4292770>
- Bouabdalli, E.M., El Jouad, M., Hajjaji, A., Touhtouh, S.: First investigation of the effect of strontium oxide on the structure of phosphate glasses using molecular dynamics simulations. *Research Square*, 1–18, 06 April (2022f) <https://doi.org/10.21203/rs.3.rs-1522777/v1>
- Brow, R.K.: The structure of simple phosphate glasses. *J. Non-Cryst. Solids* 263–264, 1–28 (2000)
- Burrill, J., Hafeli, U., Liu, D.M.: Advances in radioembolization-Embolics and isotopes. *J. Nucl. Med. Radiat. Ther.* **2**(1), 107 (2011). <https://doi.org/10.4172/2155-9619.1000107>
- Cochran, K.W., Doull, J., Mazur, M., DuBois, K.P.: Acute toxicity of zirconium, columbium, strontium, lanthanum, cesium, tantalum and yttrium. *Arch. Indust Hyg. Occup. Med.* **1**(6), 637–650 (1950)
- Deepa, A.V., Priya Murugasen, P., Muralimanohar, P., Praveen Kumar, S.: Optical studies of lanthanum oxide doped phosphate glasses. *Optik* **16**, 348–352 (2018). <https://doi.org/10.1016/j.ijleo.2018.01.108>
- Dejneka, M., Snitzer, E., Riman, R.E.: Blue, green and red fluorescence and energy transfer of Eu^{3+} in fluoride glasses. *J. Lumin.* **65**(5), 227–245 (1995). [https://doi.org/10.1016/0022-2313\(95\)00073-9](https://doi.org/10.1016/0022-2313(95)00073-9)
- Devidas, G.B., Sankarappa, T., Prashant Kumar, M., Kumar, S.: AC conductivity in rare earth ions doped vanadophosphate glasses. *J. Mater. Sci.* **43**, 4856–4861 (2008). <https://doi.org/10.1007/s10853-008-2705-z>
- Dimitrov, V., Komatsu, T.: Effect of interionic interaction on the electronic polarizability, optical basicity and binding energy of simple oxides. *J. Ceram. Soc. Jpn.* **107**(11), 1012–1018 (1999). <https://doi.org/10.2109/jcersj.107.1012>
- Dimitrov, V., Sakka, S.: Electronic oxide polarizability and optical basicity of simple oxides. I. *J. Appl. Phys.* **79**(3), 1736–1740 (1996). <https://doi.org/10.1063/1.360962>
- Doweidar, H., Moustafa, Y.M., El-Egili, K., Abbas, I.: Infrared spectra of Fe_2O_3 - PbO - P_2O_5 glasses. *Vib. Spectrosc.* **37**(1), 91–96 (2005). <https://doi.org/10.1016/j.vibspec.2004.07.002>
- DuBois, K.P.: Chemical toxicity of salts of lanthanum, yttrium and some other rare metals to Animals. *Rare Earths Biochem. Med. Res. ORINS* **12**, 91–98 (1956)
- Duffy, J.A.: Optical basicity of Titanium(IV) oxide and Zirconium(IV) oxide. *J. Am. Ceram. Soc.* **72**(10), 2012–2013 (1989). <https://doi.org/10.1111/j.1151-2916.1989.tb06022.x>
- Duffy, J.A., Ingram, M.D.: Establishment of an optical scale for lewis basicity in inorganic oxyacids, molten salts, and glasses. *J. Am. Chem. Soc.* **93**(24), 6448–6454 (1971). <https://doi.org/10.1021/ja00753a019>
- El Jouad, M., Bouabdalli, E.M., Touhtouh, S., Addou, M., Ollier, N., Sahraoui, B.: Red luminescence and UV light generation of europium doped zinc oxide thin films for optoelectronic applications. *EPJ Appl. Phys.* **91**(1), 10501 (2020). <https://doi.org/10.1051/epjap/2020200133>

- Bouabdalli, E.M., El Jouad, M., Touhtouh, S., Sadek, O., Hajjaji, A.: Structural studies on varied concentrations of europium doped strontium phosphate glasses. *Mater. Today Proc.* **66**, 349–352 (2022h). <https://doi.org/10.1016/J.MATPR.2022.05.450>
- Elbatal, H.A., Abdelghany, A.M., Ghoneim, N.A., Elbatal, F.H.: Effect of 3d-transition metal doping on the shielding behavior of barium borate glasses: a Spectroscopic Study. *Spectrochim. Acta Part A Mol. Biomol. Spectrosc.* **133**, 534–541 (2014). <https://doi.org/10.1016/j.saa.2014.06.044>
- El-Mallawany, R., Dirar Abdalla, M., Abbas Ahmed, I.: New tellurite glass: optical properties. *Mater. Chem. Phys.* **109**(2–3), 291–296 (2008). <https://doi.org/10.1016/j.matchemphys.2007.11.040>
- El-Rehim, A.F.A., Wahab, E.A.A., Halaka, M.M.A., Shaaban, K.S.: Optical properties of SiO₂ – TiO₂ – La₂O₃ – Na₂O – Y₂O₃ glasses and a novel process of preparing the parent glass-ceramics. *SILICON* (2022). <https://doi.org/10.1007/s12633-021-01002-w>
- Erbe, E.M., Day, D.E.: Chemical durability of Y₂O₃-Al₂O₃-SiO₂ glasses for the in vivo delivery of beta radiation. *J. Biomed. Mater. Res.* **27**(10), 1301–1308 (1993). <https://doi.org/10.1002/jbm.820271010>
- Fayad, A.M., Abd-Allah, W.M., Moustafa, F.A.: Effect of gamma irradiation on structural and optical investigations of borosilicate glass doped yttrium oxide. *SILICON* **10**(3), 799–809 (2018). <https://doi.org/10.1007/s12633-016-9533-6>
- Fu, Y., Christie, J.K.: Atomic structure and dissolution properties of yttrium-containing phosphate glasses. *Int. J. Appl. Glass Sci.* **8**(4), 412–417 (2017). <https://doi.org/10.1111/ijag.12325>
- Gedam, R.S., Ramteke, D.D.: Electrical, dielectric and optical properties of La₂O₃ doped lithium borate glasses. *J. Phys. Chem. Solids* **74**(7), 1039–1044 (2013). <https://doi.org/10.1016/J.JPCS.2013.03.001>
- Hager, I.Z., El-Mallawany, R.: Preparation and structural studies in the (70–x) TeO₂-20WO₃-10Li₂O-XLn₂O₃ Glasses. *J. Mater. Sci.* **45**(4), 897–905 (2010)
- Halimah, M.K., Azuraida, A., Ishak, M., Hasnimulyati, L.: Influence of bismuth oxide on gamma radiation shielding properties of Boro-Tellurite glass. *J. Non-Cryst. Solids* **512**, 140–147 (2019). <https://doi.org/10.1016/J.JNONCRY SOL.2019.03.004>
- Hyatt, M.J., Day, D.E.: Glass properties in the yttria-alumina-silica system. *J. Am. Ceram. Soc.* **70**(10), C-283 (1987). <https://doi.org/10.1111/j.1151-2916.1987.tb04901.x>
- Inaba, S., Fujino, S., Morinaga, K.: Young's modulus and compositional parameters of oxide glasses. *J. Am. Ceram. Soc.* **82**(12), 3501–3507 (1999). <https://doi.org/10.1111/j.1151-2916.1999.tb02272.x>
- Karaçoban, B., Özdemir, L.: Transition parameters for doubly ionized lanthanum. *J. Atomic Mol. Opt. Phys.* **2012**, 1–15 (2012). <https://doi.org/10.1155/2012/246105>
- Kaur, G., Kumar, M., Arora, A., Pandey, O.P., Singh, K.: Influence of Y₂O₃ on structural and optical properties of SiO₂-BaO-ZnO-xB₂O₃-(10-x) Y₂O₃ glasses and glass ceramics. *J. Non-Cryst. Solids* **357**(3), 858–863 (2011). <https://doi.org/10.1016/j.jnoncrysol.2010.11.103>
- Kawashita, M., Matsui, N., Li, Z., Miyazaki, T.: Novel synthesis of yttrium phosphate microspheres for radioembolization of cancer. In: IOP Conference Series: Materials Science and Engineering **18** (2011)
- Lai, Y.M., Liang, X.F., Yang, S.Y., Wang, J.X., Zhang, B.T.: Raman spectra study of iron phosphate glasses with sodium sulfate. *J. Mol. Struct.* **1013**, 134–137 (2012). <https://doi.org/10.1016/J.MOLSTRUC.2012.01.025>
- Li, G., Zhang, C., Song, P., Zhu, P., Zhu, K., He, J.: Luminescence properties in Tb³⁺/Yb³⁺ codoped phosphate glasses for solar cells. *J. Alloys Compd* **662**, 89–93 (2016). <https://doi.org/10.1016/j.jallcom.2015.12.074>
- Li, H., Yi, J., Qin, Z., Sun, Z., Xu, Y., Wang, C., Zhao, F., Hao, Y., Liang, X.: Structures, thermal expansion, chemical stability and crystallization behavior of phosphate-based glasses by influence of rare earth. *J. Non-Cryst. Solids* **522**, 119602 (2019). <https://doi.org/10.1016/J.JNONCRY SOL.2019.119602>
- Liang, X., Yin, G., Yang, S., Lai, Y., Wang, J.: Lanthanum oxide effects on the structure of calcium phosphate glasses. *Spectrosc. Lett.* **44**(6), 418–423 (2011)
- Lide, D.R.: *CRC Handbook of Chemistry and Physics*, vol. 85. CRC Press, Florida (2004)
- Linganna, K., Jayasankar, C.K.: Optical properties of Eu³⁺ ions in phosphate glasses. *Spectrochim. Acta Part A Mol. Biomol. Spectrosc.* **97**, 788–797 (2012). <https://doi.org/10.1016/J.SAA.2012.07.031>
- Lu, M., Wang, Fu., Liao, Q., Chen, K., Qin, J., Pan, S.: FTIR spectra and thermal properties of TiO₂-doped iron phosphate glasses. *J. Mol. Struct.* **1081**, 187–192 (2015). <https://doi.org/10.1016/j.molstruc.2014.10.029>
- Mahdi Bouabdalli, E., El Jouad, M., Hajjaji, A., Garmim, T., Touhtouh, S.: Synthesis and characterization of silicophosphate glasses doped with europium. *Mater. Today Proc.* **66**, 158–161 (2022). <https://doi.org/10.1016/J.MATPR.2022.04.299>
- Makhkhas, Y., Aqdim, S., Sayouty, E.H.: Study of sodium-chromium-iron-phosphate glass by XRD, IR, chemical durability and SEM. In: *Technical Proceedings of the 2013 NSTI Nanotechnology Conference and Expo, NSTI-Nanotech 2013* **1** (2013)

- Mariscal-Becerra, L., Carmona-Téllez, S., Arredondo-Martínez, G.V., Salas-Mariscal, S., Hernández-Sánchez, J., Murrieta, H., Falcony, C.: Yttrium-europium oxide doped zinc phosphate glasses, a luminescence study. *J. Non-Cryst. Solids* **471**, 268–273 (2017). <https://doi.org/10.1016/j.jnoncrysol.2017.06.003>
- Mohan, S., Thind, K.S., Sharma, G.: Effect of Nd³⁺ concentration on the physical and absorption properties of sodium-lead-borate glasses. *Braz. J. Phys.* **37**(4), 1306–1313 (2007). <https://doi.org/10.1590/s0103-97332007000800019>
- Moss, T.S.: Relations between the refractive index and energy gap of semiconductors. *Phys. Status Solidi (b)* **131**(2), 415–427 (1985)
- Naftaly, M., Miles, R.E.: Terahertz time-domain spectroscopy of silicate glasses and the relationship to material properties. *J. Appl. Phys.* **102**(4), 043517 (2007). <https://doi.org/10.1063/1.2771049>
- Novatski, A., Steimacher, A., Medina, A.N., Bento, A.C., Baesso, M.L., Andrade, L.H.C., Lima, S.M., Guyot, Y., Boulon, G.: Relations among nonbridging oxygen, optical properties, optical basicity, and color center formation in CaO-MgO aluminosilicate glasses. *J. Appl. Phys.* **104**(9), 094910 (2008). <https://doi.org/10.1063/1.3010306>
- Omar, N.A., Sheh, Y.W., Fen, K.A., Matori, M.H., Zaid, M., Samsudin, N.F.: Structural and optical properties of Eu³⁺ activated low cost zinc soda lime silica glasses. *Res. Phys.* **6**, 640–644 (2016). <https://doi.org/10.1016/J.RINP.2016.09.007>
- Rada, S., Chelcea, R., Culea, E.: Experimental and theoretical investigations on the structure-properties interrelationship of the gadolinium-vanadate-germanate glasses. *J. Mol. Model.* **17**, 165–171 (2011). <https://doi.org/10.1007/s00894-010-0706-8>
- Rada, M., Culea, E., Rada, S., Bot, A., Aldea, N., Rednic, V.: Anomalies of some physical properties and electrochemical performance of lithium-lead-germanate glasses. *J. Non-Cryst. Solids* **358**(23), 3129–3136 (2012). <https://doi.org/10.1016/J.JNONCRY SOL.2012.08.026>
- Ramesh, R., Nestor, E., Pomeroy, M.J., Hampshire, S.: Formation of Ln-Si-Al-O-N glasses and their properties. *J. Eur. Ceram. Soc.* **17**(15–16), 1933–1939 (1997). [https://doi.org/10.1016/s0955-2219\(97\)00057-5](https://doi.org/10.1016/s0955-2219(97)00057-5)
- Rammah, Y.S., Kilic, G., El-Mallawany, R., Issever, U.G., El-Agawany, F.I.: Investigation of optical, physical, and gamma-ray shielding features of novel vanadyl boro-phosphate Glasses. *J. Non-Cryst. Solids* **533**, 119905 (2020). <https://doi.org/10.1016/J.JNONCRY SOL.2020.119905>
- Ramzi, Z., Touhtouh, S., Nachit, W., Benkhouja, K., Taibi, M.H., Hajjaji, A.: Investigation of structural and physical properties of xSrO-(100-x) P₂O₅ glasses. *Mol. Cryst. Liq. Cryst.* **627**(1), 97–105 (2016). <https://doi.org/10.1080/15421406.2015.1137137>
- Riaz, A., Lewandowski, R.J., Kulik, L., Salem, R.: Yttrium-90 Radioembolization using therasphere® in the management of primary and secondary liver tumors. *Q. J. Nucl. Med. Mol. Imaging* **53**(3), 311 (2009)
- Riaz, A., Kulik, L.M., Mulcahy, M.F., Lewandowski, R.J., Salem, R.: Yttrium-90 radioembolization in the management of liver malignancies. *Semin. Oncol.* **37**(2), 94–101 (2010). <https://doi.org/10.1053/j.seminoncol.2010.03.006>
- Rulmont, A., Cahay, R., Liegeois-Duyckaerts, M., Tarte, P.: Vibrational spectroscopy of phosphates: some general correlations between structure and spectra. *Eur. J. Solid State Inorg. Chem.* **28**(1), 207–219 (1991)
- Sadek, O., Touhtouh, S., Bouabdalli, E.M., Hajjaji, A.: Development of a protocol for the rapid identification of solid materials using the principal component analysis (ACP) method: case of phosphate fertilizers. *Mater. Today: Proc.* **66**, 402–407 (2022). <https://doi.org/10.1016/J.MATPR.2022.06.083>
- Salem, R., Hunter, R.D.: Yttrium-90 microspheres for the treatment of hepatocellular carcinoma: a review. *Int. J. Radiat. Oncol. Biol. Phys.* **66**(SUPPL 2), S83–S88 (2006). <https://doi.org/10.1016/j.ijrobp.2006.02.061>
- Schena, E., Saccomandi, P., Fong, Y.: Laser ablation for cancer: past, present and future. *J. Funct. Biomater.* **8**(2), 19 (2017). <https://doi.org/10.3390/jfb8020019>
- Schubert, D., Dargusch, R., Raitano, J., Chan, S.W.: Cerium and yttrium oxide nanoparticles are neuro-protective. *Biochem. Biophys. Res. Commun.* **342**(1), 86–91 (2006). <https://doi.org/10.1016/j.bbrc.2006.01.129>
- Sene, F.F., Martinelli, J.R., Gomes, L.: Synthesis and characterization of niobium phosphate glasses containing barium and potassium. *J. Non-Cryst. Solids* **348**, 30–37 (2004)
- Sene, F.F., Martinelli, J.R., Okuno, E.: Synthesis and characterization of phosphate glass microspheres for radiotherapy applications. *J. Non-Cryst. Solids* **354**(42–44), 4887–4893 (2008). <https://doi.org/10.1016/j.jnoncrysol.2008.04.041>

- Shaaban, K.S., Wahab, E.A.A., Shaaban, E.R., Yousef, E.S., Mahmoud, S.A.: Electronic polarizability, optical basicity and mechanical properties of aluminum lead phosphate glasses. *Opt. Quantum Electron.* **52**(2), 1–16 (2020). <https://doi.org/10.1007/s11082-020-2191-3>
- Shajan, D., Murugasen, P., Sagadevan, S.: Studies on structural, optical and spectral properties of europium oxide doped phosphate glasses. *Optik* **136**, 165–171 (2017). <https://doi.org/10.1016/j.ijleo.2017.02.013r>
- Shih, P.Y.: Thermal, chemical and structural characteristics of erbium-doped sodium phosphate glasses. *Mater. Chem. Phys* 1–6 (2004). <https://doi.org/10.1016/j.matchemphys.2003.11.016>
- Sidek, H.A.A., Senin, H.B., Saunders, G.A., Ball, D., Cankurtaran, M., Federico, M.: Elastic, anelastic and nonlinear acoustic properties of $(ZnCl_2)_x (P_2O_5)_{1-x}$ glasses. *Phys. Chem. Glasses* **39**(1), 17–22 (1998)
- Sidek, H., Chow, S.P., Talib, Z.A., Halim, S.A.: Formation and elastic behavior of lead-magnesium chlorophosphate glasses. *Turk. J. Phys.* **28**(1), 65–72 (2004)
- Silva, A.M.B., Correia, R.N., Oliveira, J.M.M., Fernandes, M.H.V.: Structural characterization of TiO_2 - P_2O_5 - CaO glasses by spectroscopy. *J. Eur. Ceram. Soc.* **30**(6), 1253–1258 (2010). <https://doi.org/10.1016/J.JEURCERAMSOC.2009.11.001>
- Simon, V., Eniu, D., Takács, A., Magyari, K., Neumannray, M., Simon, S.: X-ray photoemission study of yttrium contained in radiotherapy systems. *J. Optoelectron. Adv. Mater.* **7**(6), 2853 (2005)
- Singh, K., Gupta, N., Pandey, O.P.: Effect of Y_2O_3 on the crystallization behavior of SiO_2 - MgO - B_2O_3 - Al_2O_3 glasses. *J. Mater. Sci.* 6426–6432 (2007). <https://doi.org/10.1007/s10853-006-1188-z>
- Singh, S., Kalia, G., Singh, K.: Effect of intermediate oxide (Y_2O_3) on thermal, structural and optical properties of lithium borosilicate glasses. *J. Mol. Struct.* 239–245 (2015). <https://doi.org/10.1016/j.molstruc.2015.01.031>
- Sreedhar, V.B., Ramachari, D., Jayasankar, C.K.: Optical properties of zincfluorophosphate glasses doped with Dy^{3+} ions. *Phys. B Condens. Matter* **408**(1), 158–163 (2013). <https://doi.org/10.1016/j.physb.2012.09.047>
- Triller, J., Baer, H.U., Geiger, L., Kinser, J., Rösler, H., Blumgart, L.H.: Radioembolisation of hepatocellular carcinoma with 90-yttrium resin particles. *Eur. Radiol.* **5**(6), 603–608 (1995). <https://doi.org/10.1007/BF00190925>
- Veeranna Gowda, V.C.: Effect of Bi^{3+} ions on physical, thermal, spectroscopic and optical properties of Nd^{3+} doped sodium borate glasses. *Phys. B Condens. Matter* **426**, 58–64 (2013). <https://doi.org/10.1016/J.PHYSB.2013.06.007>
- Waring, R.K., Hsu, W.Y.: Urbach rule behavior in strongly absorbing fine particle solids. *J. Appl. Phys.* **54**(7), 4093–4096 (1983). <https://doi.org/10.1063/1.332541>
- Yakuphanoglu, F.: Electrical characterization and device characterization of ZnO microring shaped films by sol-gel method. *J. Alloys Compd.* **507**(1), 184–189 (2010). <https://doi.org/10.1016/J.JALLCOM.2010.07.151>
- Zheng, J., Zhongqing Liu, Xu., Liu, X.Y., Li, D., Chu, W.: Facile hydrothermal synthesis and characteristics of B-Doped TiO_2 hybrid hollow microspheres with higher photo-catalytic activity. *J. Alloys Compd.* **509**(9), 3771–3776 (2011). <https://doi.org/10.1016/J.JALLCOM.2010.12.152>

Publisher's Note Springer Nature remains neutral with regard to jurisdictional claims in published maps and institutional affiliations.

Springer Nature or its licensor (e.g. a society or other partner) holds exclusive rights to this article under a publishing agreement with the author(s) or other rightsholder(s); author self-archiving of the accepted manuscript version of this article is solely governed by the terms of such publishing agreement and applicable law.